

Peak Power Minimization for Commercial Thermostatically Controlled Loads in Multi-Unit Grid-Interactive Efficient Buildings

Syed Ahsan Raza Naqvi*, Koushik Kar*, Saptarshi Bhattacharya† and Vikas Chandan‡

*Rensselaer Polytechnic Institute, Troy, NY, USA, †Pacific Northwest National Laboratory, Richland, WA, USA.

Email: naqvis2@rpi.edu, koushik@ecse.rpi.edu, saptarshi.bhattacharya@pnnl.gov, vikas.chandan@pnnl.gov

Abstract—The load profiles of most commercial and industrial consumers are characterized by brief periods of very high power consumption followed by intervals of lower demand. To encourage such consumers to flatten their load profiles, power utilities around the world often levy a monthly demand charge (DC) on the peak demand measured over brief intervals. In this work, we consider the joint optimization of energy costs (EC) and the instantaneous peak power of a multi-unit building which uses a hydronic heating, ventilation and air-conditioning (HVAC) system and responds to a demand response (DR) program. Despite the apparent non-convexity of the control framework, we show how it may be transformed into a convex optimization problem. Next, we study the power demand patterns resulting from our proposed strategy for thermostatically controlled loads (TCLs), and evaluate the strategy’s performance for various climate zones in the US under both typical and atypical weather conditions. The results show that, depending on the ambient conditions and the tariff structure, our strategy can result in utility bill savings of up to nearly 19% compared to the baseline. The results also indicate that our power control strategy can significantly reduce the instantaneous peak power consumption in commercial TCLs.

Keywords—demand charge, demand response, thermostatically controlled loads.

I. INTRODUCTION

It has been estimated [1] that nearly 30% of the total energy consumed by the commercial building sector in the United States in 2017 was due to heating, ventilation and air-conditioning (HVAC) systems. Ambient temperatures during the summer in the US can often exceed 40°C in some regions, causing an increase in the demand for electricity for space cooling. In response, system operators have to increase power generation which is often achieved by dispatching peaking power plants. In addition to being expensive to operate, these plants also have an adverse impact on the environment. The elevated operation costs for such plants result in higher energy prices for the consumers. Therefore, there is a need to develop energy efficient power control policies for HVAC operations in modern buildings.

Commercial loads are often characterized by brief periods of very high power consumption. In order to cover the cost of maintaining the infrastructure for delivering such high power [2], electric utilities in the US and Europe levy a demand charge (DC) tariff on commercial consumers based on the

their peak power demand during the month. Past studies have ascertained that effective implementation of building HVAC controls can reduce power consumption by over 20% [3]. It has also been shown that 10–20% of the peak load in commercial buildings can be temporarily managed or curtailed to provide grid services [4]. Demand response (DR) in buildings can help flatten consumer load profiles.

Hydronic HVAC systems, which use water to provide indoor heating/cooling, have become increasingly popular with commercial building operators due to their energy efficiency and potential for off-peak storage [5]. Through this paper, we aim to develop a rapidly deployable power control strategy for a grid-interactive efficient building (GEB) [6] that uses a hydronic HVAC system and is *DR-amenable*. Here, we define *DR-amenability* as the practice of permitting indoor temperatures to vary within a thermal dead-band. Due to the slow thermodynamics of buildings, for a suitable control strategy, heating/cooling loads can be shifted or curtailed, at the cost of some thermal discomfort to the occupants [7]. We develop a power control strategy for commercial heating/cooling that minimizes both the peak power consumption and the energy cost (EC).

In this work, we consider a hydronic HVAC system serving a multi-unit commercial building to meet indoor heating/cooling requirements, as shown in Fig. 1. We develop an optimal control strategy that minimizes the EC and the peak power consumption of a DR-amenable, multi-unit commercial building. Adjacent units are taken to be thermally coupled. Therefore, we not only take into consideration the heat transfer between a unit and the outside environment, but also that between adjoining units. We assume that the DR program allows the indoor temperatures to deviate within a thermal dead-band, as agreed upon by the building operator and the power utility. Finally, we simulate our model to determine the optimal electrical power required to achieve the desired heating/cooling in individual units. Preliminary results for our proposed approach for selected climate zones prevalent in the US were presented in [8]. These initial results show that our solution has a strong potential for saving significant energy-related expenditures for DR-amenable commercial buildings. In this paper, we use our control framework to expand upon the existing results to provide an exhaustive performance evaluation for all climate zones present in the US. We further

study the efficacy of our approach for anomalous weather patterns, as represented by the unusually low winter temperatures experienced in Austin, TX, in Feb. 2021. Unlike [8], we assess the performance of our proposed approach for both heating and cooling demands.

In the context of peak power reduction for thermostatically controlled loads (TCLs), our contributions are:

- We develop an optimization framework that jointly minimizes the EC and the instantaneous peak power for a GEB equipped with a *hydronic* HVAC system. For our study, we take into account both the heat transfer to/from the external surroundings as well as that through shared walls inside the building. The achievable peak power reduction indicates that a large-scale deployment of our control policy can potentially reduce the maintenance and operational costs of the power delivery infrastructure, which may otherwise be adversely affected by large intermittent loads.
- In spite of the apparent non-convexity of the control framework, we show how the multi-unit thermal regulation problem can be given by a single vector of unknowns and subsequently solved using linear optimization method. This reduced dimensionality makes the approach scalable for large-scale deployment as GEBs have limited on-site computational resources. This, in turn, ensures operational convenience for the practitioner. Through this work, we have shown that our proposed framework scales well for an increasing number of indoor spaces. To the best of the authors' knowledge, this work is the first attempt to develop an optimization framework for minimizing EC and peak power consumption for hydronic HVAC systems.
- We study the performance of our control policy for both heating and cooling loads. We also compare its performance under typical weather conditions along with atypical, extreme weather events. To the best of the authors' knowledge, this paper is the first in its domain to present a detailed performance evaluation of an optimization framework for an HVAC system for the different climate zones and tariff structures in the US.
- We determine the effect of changing the relative weights of the EC and the instantaneous peak power on energy consumption and the total payable utility bill. In doing so, we have been able to determine the range of weights that the practitioner could adopt to achieve savings in the utility bill.

The rest of this paper is organized as follows. Section II is a review of the existing literature relevant to our work. Section III offers details on the system model and casts our proposed approach as a minimization problem. Section IV provides a mathematical analysis of the problem. Section V presents a discussion on the simulation results. Section VI is a summary of this paper. The details of mathematical derivations may be found in [29].

II. LITERATURE REVIEW

A considerable amount of recent research has studied the use of TCLs to provide ancillary services to the power grid ([9], [10]), especially under increased penetration of renewable energy resources [11]. Similarly, related literature has also studied various aspects of implementing DR for TCLs. The authors in [7] aimed to determine the potential of employing DR programs for residential HVAC systems. The DR strategy was implemented using a thermal dead-band based on the occupants' tolerance to changes in the indoor temperature. In contrast to our work, the authors in [7] did not take into account the significance of energy prices in the implementation of DR, nor did they aim to control the peak power consumption.

The papers [12], [13] considered an integrated community energy systems operator that supplies energy for meeting the heating requirements of a collection of DR-amenable buildings equipped with hydronic HVAC systems. The authors formulated a bi-level optimization problem whereby the operator wished to maximize its profits and the buildings aimed to minimize their energy costs while meeting their heating requirements. While the building-side control was actuated by varying the mass flow rate of water to individual units, the paper considered the temperature of the returning water in each building to be known and constant. In contrast, our proposed framework takes into account the disparity in the temperatures of the water returning from individual units in a building, which introduces substantial complexity to the formulation. The authors in [14] developed a two-stage HVAC load scheduling model for residential buildings. Unlike [14], we consider a *multi-unit* commercial building with thermally coupled indoor spaces. Also, in contrast to [14], we consider a commercial load and minimize both EC and instantaneous peak power.

Peak load minimization in HVAC systems has also received significant attention recently. For instance, in [15] the authors developed a grey-box model for determining the temperature evolution in a test-bed. The approach combined thermodynamics with data analytics to characterize the parameters of the test-bed's thermal model. The authors used this model to determine the optimal pre-cooling for the indoor space to achieve a desired set-point range. Subsequently, an upper bound was imposed on the instantaneous power consumed to restrict the DC. Unlike [15], we develop a model predictive control (MPC)-based power control policy for a *multi-unit* commercial building served by a *hydronic* HVAC system. Furthermore, instead of imposing a constraint on the total instantaneous power consumed, we incorporate the peak demand into our objective function.

In [16], the authors formulated a bi-layer optimization framework for a variable air volume (VAV) HVAC system to simultaneously minimize the thermal discomfort, EC and the DC. In [17], the authors considered the problem of co-scheduling data-center and HVAC loads, in the presence of solar energy and battery storage. The proposed control strategy

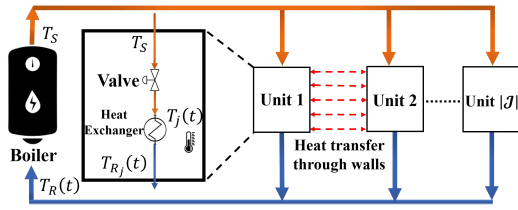


Fig. 1: Representation of the hydronic HVAC system considered in this paper (heating operation).

aimed to minimize building EC and the DC while satisfying constraints on room temperature and data-center workload deadlines. Unlike our work, [17] only considered isolated, non-adjacent indoor spaces for temperature regulation. Both [16] and [17] used an MPC-based approach to meet their control objectives. However, unlike the aforementioned papers, we demonstrate how the optimization framework for multi-unit thermal regulation can be expressed in terms of a single vector of unknowns, resulting in linear constraints. Since our work considers a hydronic HVAC system (unlike [16] and [17] which consider a VAV HVAC system), our optimization framework is also expressed in terms of the temperature of the water returning from individual units, which significantly increases the mathematical complexity of the optimization problem we hope to solve through this work. Moreover, neither [16] nor [17] claimed to provide globally optimum solutions to the EC and peak power minimization problem. Our work, in contrast, shows that such an optimization framework can indeed be cast as a convex optimization problem.

In [18], the authors used a minmax optimization technique to minimize the peak power usage in a DR-amenable building. The control variables in the resulting optimization problem included, among other quantities, the mass flow rate of water and the room temperature set-point. Due to the numerous control variables involved, scaling this approach to several buildings is challenging. In contrast, our work uses an approach that expresses the peak power minimization problem in terms of only the power consumed over a time horizon. While the existing body of work has extensively studied the optimization of HVAC operations, there is a need to develop a rapidly deployable power control strategy for GEBs and to ascertain its efficacy under various demand scenarios. We aim to address this gap through this paper.

Some aspects of the theoretical framework used in this work were developed in one of our earlier papers [19]. It expressed the optimization problem for minimizing the weighted sum of the thermal discomfort and the EC in terms of the power consumed by individual units. However, the indoor units in the building considered in [19] were not thermally coupled, as is the case in this paper. Since the framework in [19] was developed for residential buildings, it did not aim to minimize the instantaneous peak power consumption (and, hence, DC) incurred by the consumer. In contrast, this paper minimizes the weighted sum of EC and the instantaneous peak power. Finally, unlike [19], we perform a detailed analysis of our control strategy across climate zones as well as anomalous weather conditions.

III. PROBLEM FORMULATION

In this work, we consider a commercial building which consists of a set of units \mathcal{J} . Each unit j has its own temperature set-point, Δ_j . We take ρ to denote the maximum permitted temperature swing about Δ_j . This thermal dead-band introduces flexibility to the HVAC load, thereby enabling the implementation of a DR program. The mass flow rate of water to individual units, based on their heating/cooling demands, is controlled by valves. We assume that the zonal temperature of each unit is spatially uniform. We employ the standard R-C model to represent the thermal characteristics of the indoor units. Since we assume that the walls connecting adjoining units are thin, they can be modeled as single resistive elements. We further assume that the buildings' thermal properties are known to (or are well-estimated by) the utility in advance. We assume the HVAC system to be 100% efficient, i.e., all the electrical power used to heat the water is converted into thermal energy for heating individual units. $P_j(t)$ is the instantaneous power required to heat unit j . Each unit has instantaneous temperature $T_j(t)$. Lastly, $P^{\text{total}}(t)$ is the total instantaneous power required to heat all the units. Although we consider a heating scenario here, our formulation and analysis are applicable to the cooling scenario as well.

The HVAC system considered here distributes heated water from a central source to spaces within a building to meet their heating demands. The central source in this case is a boiler running on electrical power. The water leaving the boiler is maintained at a constant temperature which is given by T_S . The individual spaces are equipped with fan coil units. The hydronic system uses valves to control the instantaneous water mass flow rate to the fan coil unit in unit j , which is denoted by $\dot{m}_j(t)$. The instantaneous temperature of the water returning to the boiler from unit j is given by $T_{R,j}(t)$. Fig. 1 is a representation of the HVAC system being studied here.

Our optimization problem minimizes the weighted sum of the total EC for the consumers and the instantaneous peak power consumed over a given time horizon. We aim to use an MPC-based approach to determine the optimal power for satisfying this objective. In mathematical terms, we minimize,

$$\alpha \int_0^\tau \pi(t) P^{\text{total}}(t) dt + (1 - \alpha) \varpi \left[\max_{0 \leq t \leq \tau} |P^{\text{total}}(t)| \right] dt, \quad (1)$$

subject to,

$$\begin{aligned} (\bar{C}_1) \dot{T}_j(t) &= \frac{1}{C_j} \left\{ \frac{1}{R_j^o} [T_\infty(t) - T_j(t)] + P_j(t) + \sum_{i \in \mathcal{B}_j} \frac{1}{R_{i,j}^w} (T_i(t) - T_j(t)) \right\}, \quad \forall j \in \mathcal{J}, \forall t \in [0, \tau], \\ (\bar{C}_2) P_j(t) &= \dot{m}_j(t) S_p(T_S - T_{R,j}(t)), \quad \forall j \in \mathcal{J}, \forall t \in [0, \tau], \\ (\bar{C}_3) P_j(t) &= h_R \left(\frac{T_S + T_{R,j}(t)}{2} - T_j(t) \right), \quad \forall j \in \mathcal{J}, \forall t \in [0, \tau], \end{aligned}$$

$$(\bar{C}_4) \dot{m}_j(t) \in \left[0, \frac{1}{\phi_j}\right], \quad \forall j \in \mathcal{J}, \forall t \in [0, \tau],$$

$$(\bar{C}_5) |T_j(t) - \Delta_j| \leq \rho, \quad \forall j \in \mathcal{J}, \forall t \in [0, \tau],$$

where α is a constant and τ is the length of the prediction window. As seen in [19], ϕ_j is a constant and $\phi_j \leq \frac{1}{\dot{m}_j(t)} < \infty$. The initial temperature of unit j is given by $T_j(0) = T_j^0$. Additionally, $\pi(t)$ represents the energy price at time t , whereas ϖ is the DC tariff. Let C_j represent the thermal capacitance of unit j . R_j^o and $R_{i,j}^w$ are the thermal resistances of the walls connecting unit j with the outside environment and with unit i , respectively. Let \mathcal{B}_j denote the set of units that share a wall with unit j . $T_\infty(t)$ is the ambient temperature at time t and is assumed to be known or well-estimated in advance. S_p is the specific heat capacity of water. T_S is the temperature of the water at the central source and is assumed to have a constant value. $T_{R,j}(t)$ is the instantaneous temperature of the water returning to the central source and h_R is the coefficient of heat exchange between water and air.

For the minimization problem in (1), (\bar{C}_1) characterizes the temporal evolution of the temperature in individual units. Constraint (\bar{C}_2) is the relationship between heat transfer and the temperature change of water. Constraint (\bar{C}_3) represents the heat transfer between water and air by convection. Here, the temperature of the water arriving at the unit is estimated to be the average of the temperatures of the supplied and returning water. Constraint (\bar{C}_4) represents the operational bounds on $\dot{m}_j(t)$. Finally, constraint (\bar{C}_5) introduces a thermal dead-band for zonal temperatures.

The instantaneous temperature of the water returning from the units to the central source is denoted by $T_R(t)$. This quantity is given by,

$$T_R(t) = \frac{\sum_{j \in \mathcal{J}} \dot{m}_j(t) T_{R,j}(t)}{\sum_{j \in \mathcal{J}} \dot{m}_j(t)}. \quad (2)$$

IV. ANALYSIS

Inspecting the constraints of the minimization problem (1), it may be observed that (\bar{C}_2) causes the problem to become non-convex. Additionally, the problem contains several variables (like $\dot{m}_j(t)$, $P_j(t)$, $T_j(t)$ and $T_{R,j}(t)$) that must be determined optimally. Since this work aims to assess the feasibility of using commercial TCLs for DR, we proceed to reformulating our problem by posing it in terms of a single control variable, $P_j(t)$. We also express $T_j(t)$ in terms of known constants and the supplied power. Through the procedure followed in [19], the constraints (\bar{C}_2) , (\bar{C}_3) and (\bar{C}_4) may be subsumed into a single inequality:

$$P_j(t) \leq G[T_S - T_j(t)], \quad (3)$$

where $G = \frac{2S_p}{\phi_j + \frac{2S_p}{h_R}}$ is a constant.

Our problem is now simplified to minimizing (1) subject to constraints (\bar{C}_1) , (\bar{C}_5) and (3) and has now been expressed in terms of two continuous variables, $T_j(t)$ (the state variable) and $P_j(t)$ (the control variable). Since $P_j(t)$ is a function

of $\dot{m}_j(t)$, this framework can be implemented by directly controlling the valve operation in each unit. In practice, the value of $\dot{m}_j(t)$, and hence $P_j(t)$, undergoes changes at specific time instances, and hence may be considered to be a discrete-time variable. Therefore, we break up the time scale for the valve operation into discrete time instances, denoted by index k and with duration μ . A total of K time instances have been considered, where $K = \frac{\tau}{\mu}$. Thus, our control variable at time instance k is $P_j(k)$. Since T_∞ evolves slowly in time, its variation during a single time instance is expected to be small. Therefore, we consider the ambient temperature to be a discrete-time variable $T_\infty(k)$.

The indoor temperature dynamics are given by,

$$\dot{\mathbf{T}}(t) = \mathbf{A}\mathbf{T}(t) + \mathbf{H}(t), \quad (4)$$

where $\mathbf{T}(t) \in \mathbb{R}^{|\mathcal{J}| \times 1}$ column vector of temperatures of the unit at time t . Furthermore, $\mathbf{H}(t) \in \mathbb{R}^{|\mathcal{J}| \times 1}$ is a column vector given by $\{\frac{1}{C_j}(\frac{T_\infty(t)}{R_j^o} + P_j(t))\}$. Lastly, $\mathbf{A} \in \mathbb{R}^{|\mathcal{J}| \times |\mathcal{J}|}$ has elements $A_{i,j}$ which are defined as, $-\frac{1}{C_j}(\frac{1}{R_j^o} + \sum_{i \in \mathcal{B}_j} \frac{1}{R_{i,j}^w})$ if $i = j$, and $\mathbb{1}_{i \in \mathcal{B}_j} \frac{1}{C_j R_{i,j}^w}$ otherwise. Here $\mathbb{1}_{i \in \mathcal{B}_j}$ is 1 if $i \in \mathcal{B}_j$ and is 0 otherwise.

It is worth noting that using time-sampled versions of $T_j(t)$ can result in substantial inaccuracies in our computations. Therefore, we express $T_j(t)$ in terms of $P_j(k)$. Taking $k = \lfloor \frac{t}{\mu} \rfloor$ and using [20], \mathbf{T} may be expressed as,

$$\mathbf{T}(t) = \mathbf{M}(t - k\mu)\mathbf{M}^{-1}(0) \prod_{n=1}^{k-1} \left(\mathbf{M}(\mu)\mathbf{M}^{-1}(0) \right) \mathbf{T}_0 + \quad (5)$$

$$\sum_{k'=0}^{k-2} \left(\prod_{n=1}^{k-k'-1} \mathbf{M}(\mu)\mathbf{M}^{-1}(0) \right) \mathbf{I} \int_0^\mu \mathbf{M}(\mu)\mathbf{M}^{-1}(s)\mathbf{H}(k') ds +$$

$$\int_0^{t-k\mu} \mathbf{M}(t - k\mu)\mathbf{M}^{-1}(s)\mathbf{H}(k-1) ds, \quad t \in [k\mu, (k+1)\mu],$$

where $\mathbf{I} \in \mathbb{R}^{|\mathcal{J}| \times |\mathcal{J}|}$ is the identity matrix, $\mathbf{T}_0 \in \mathbb{R}^{|\mathcal{J}| \times 1}$, with element T_j^0 , denotes the temperature in all units at the beginning of the prediction horizon and $\mathbf{M}(t) \in \mathbb{R}^{|\mathcal{J}| \times |\mathcal{J}|}$ is the fundamental matrix for the system, $\dot{\mathbf{T}}(t) = \mathbf{A}\mathbf{T}(t)$. The matrix \mathbf{M} is defined as:

$$\mathbf{M} = \left[\lambda_1 \mathbf{v}_1 \dots \lambda_{|\mathcal{J}|} \mathbf{v}_{|\mathcal{J}|} \right], \quad (6)$$

where λ_e and \mathbf{v}_e are the e^{th} eigenvalue and eigenvector, respectively, of matrix \mathbf{A} . The objective function and the constraints can now be expressed as,

$$\alpha \sum_{k=1}^K \{ \mu \pi(k) P^{\text{total}}(k) \} + (1 - \alpha) \varpi \left[\max_{0 \leq k \leq K} |P^{\text{total}}(k)| \right], \quad (7)$$

subject to,

$$\begin{aligned}
 (C_1) \quad & |T_j(k\mu) - \Delta_j| \leq \rho, \quad \forall j \in \mathcal{J}, k \in [0, K], \\
 (C_2) \quad & P_j(k) \leq G[T_S - T_j(k\mu)], \quad \forall j \in \mathcal{J}, k \in [0, K], \\
 (C_3) \quad & (5), \quad k \in [0, K].
 \end{aligned}$$

Based on the preceding mathematical manipulations, it may be noted that the solution to the original problem in (1) can be uniquely recovered from the convex formulation (7). Henceforth, we will refer to (7) as the *energy costs plus peak demand charge minimization* (ECDCM) problem. The objective (7) and its constraints have now been expressed in terms of, and are linear in, the discrete variable $P_j(k)$, with all the other time-dependent variables being eliminated. Once the optimal values for $P_j(k)$ have been determined for all $k \in [1, K]$, (5) may be used to determine the instantaneous temperatures of individual units.

In addition to the optimization framework presented earlier, we also consider an alternative EC and peak power minimization approach to serve as a benchmark strategy for comparison. This strategy is based on the bi-layer approach presented in [16]. It is noteworthy, however, that [16] developed its control strategy for a VAV HVAC system. Therefore, we have modified the approach presented therein so that it may be applicable to the hydronic HVAC system studied in this paper. Henceforth, we will refer to this bi-layer approach as the modified autonomous hierarchical control (m-AHC) strategy.

The upper layer of the m-AHC strategy involves minimizing,

$$(7), \text{ subject to, } (C_1), (C_2), \text{ and } (4), \text{ where } \dot{\mathbf{T}}(t) = 0. \quad (8)$$

As in [16], the upper layer of the m-AHC approach obtains the temperature set-points at the steady state, $T_j^{SS}(\cdot), \forall j, k$, that minimize (7). The lower layer then minimizes,

$$\sum_{k=1}^K \sum_{j \in \mathcal{J}} \left(T_j(k\mu) - T_j^{SS}(k\mu) \right)^2, \quad (9)$$

subject to linearized thermal dynamics. The control variables in the lower layer are $P_j(k), \forall j, k$.

V. NUMERICAL STUDY

We now present simulation results to determine the power required to maintain unit temperatures within permitted bounds. We use an MPC-based approach to solve for the optimal power consumption in the building. Each unit is constrained to use a maximum power of 3 kW at any given time for cooling operations and 5 kW for heating operations. It is assumed that the commercial building operator follows a DR program whereby $\rho = 1^\circ\text{C}$ for the interval when the building is occupied (between 0800 hrs and 1800 hrs). For the rest of the day, ρ is taken to be 2°C . The baseline case is $\rho = 0^\circ\text{C}$, i.e., when DR is not implemented. Table I lists the values of the remaining simulation parameters.

A. Description of the Test-bed

We evaluate the performance of our power control strategy using a six-unit indoor space model based on our testing

TABLE I: Parameter values used in simulations.

| Parameter | Value | Parameter | Value |
|-----------------------|--------------------------|---------------------|-------------------------------------|
| T_S (cooling) | 12°C | μ | 1 min. |
| T_S (heating) | 80°C | $\phi_j, \forall j$ | $1 \text{ kg}^{-1} \text{ s}$ |
| S_p | 4200 J kg^{-1} | h_R | $5 \text{ kW } ^\circ\text{C}^{-1}$ |
| $\Delta_j, \forall j$ | 20°C | $T_j^0, \forall j$ | 21°C |

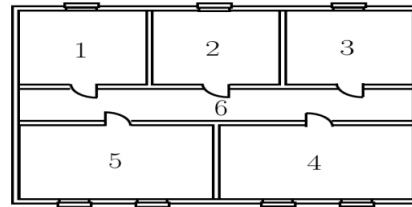


Fig. 2: Layout of the test-bed [22].

facility located in Watervliet, NY (see Fig. 2). The test-bed consists of five rooms and a corridor, representing a typical office-space. Further details of the structure and its thermal properties may be found in [21].

B. Performance Evaluation under Typical and Atypical Weather Conditions (Heating Operation)

In Feb. 2021, the state of Texas experienced unprecedented winter temperatures causing heating demands to rise sharply, which, in turn, caused the energy prices to skyrocket. In this subsection, we study how the heating operations inside a commercial building, as represented by Fig. 2, would be modified under the ECDCM strategy when it is exposed to unusually low ambient temperatures. We use the weather conditions and hourly energy prices for Austin, TX, as observed on Feb. 14th, 2021, to represent an extreme weather event. For comparative simulations, we use the corresponding data for Feb. 14th, 2020 to represent a typical winter day in Austin, TX. Fig. 3 presents the ambient weather conditions considered here for the two cases. The value of ϖ in this study is \$4.19. We assume that the commercial building is equipped with an electric boiler and that the tariffs are known (or are well-estimated) in advance.

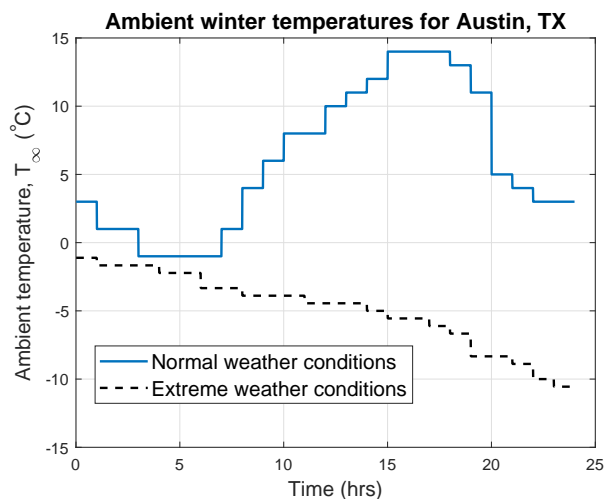


Fig. 3: Ambient temperatures for normal and extreme weather conditions during winters in Austin, TX.

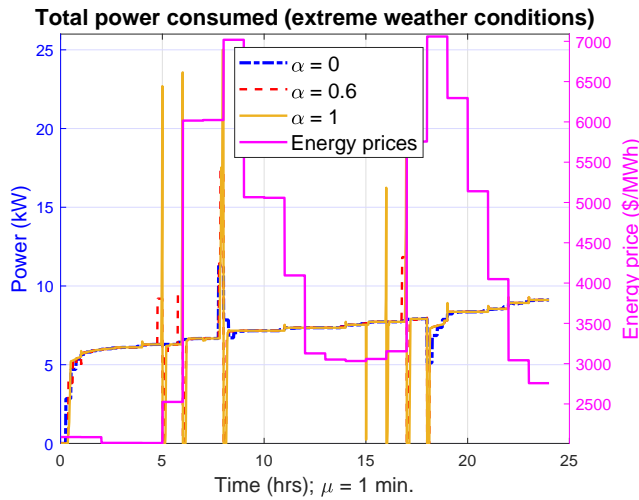


Fig. 4: Total power consumed by the building for $\alpha = 0$, $\alpha = 0.6$ and $\alpha = 1$ under extreme weather conditions and the hourly energy pricing signals.

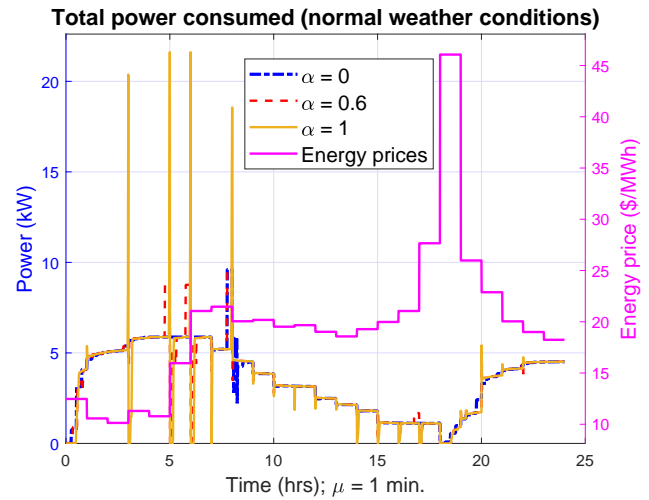


Fig. 6: Total power consumed by the building for $\alpha = 0$, $\alpha = 0.6$ and $\alpha = 1$ under normal weather conditions and the hourly energy pricing signals.

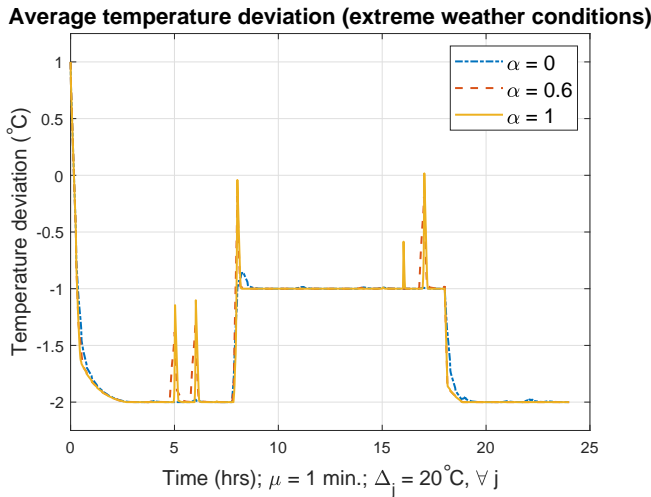


Fig. 5: Deviation from the temperature set-point for $\alpha = 0$, $\alpha = 0.6$ and $\alpha = 1$ under extreme weather conditions, averaged for all six units in the commercial building.

Fig. 4 shows the power consumption in the commercial building over a 24-hour period under extreme weather conditions for $\alpha = 0$, $\alpha = 0.6$ and $\alpha = 1$. We use $\alpha = 0$ to represent the scenario where only the instantaneous peak power is minimized. When α is set to 1, only the ECs incurred by the consumer are minimized. Finally, $\alpha = 0.6$, represents a compromise between EC and peak power reduction. The value of the total power consumed by the six units is sampled at 1-minute intervals. It may be seen in Fig. 4 that the power consumption for heating steadily increases between 0000 hrs and 0500 hrs as the ambient temperature progressively decreases during this period while the price signal remains fairly steady. In the hours immediately succeeding 0500 hrs, there is a steep increase in energy prices. In order to reduce energy consumption during high-price periods, the ECDCM strategy under $\alpha = 0$ and $\alpha = 0.6$ pre-heats the commercial building, allowing the power consumption in subsequent time instances to drop to approximately 0 kW. The pre-heating operation is characterized by a sharp jump in power consumption. This

jump is more significant for $\alpha = 0$ (the power consumption increases beyond 20 kW) than $\alpha = 0.6$. Since $\alpha = 1$ only minimizes the instantaneous sum of power consumed by all units, it does not exhibit any pre-heating operation. The curves for all three values of α demonstrate an increase in power consumption (to varying degrees) at 0800 hrs when the commercial building is taken to be occupied, with ρ reducing to 1°C from 2°C. With the ambient temperature progressively decreasing, the total power consumed by the commercial building also increases. At 1800 hrs, when ρ reverts to 2°C, all three curves exhibit a drop in the power consumption.

Fig. 5 shows the average deviation from Δ_j in the commercial building over a 24-hour period under extreme weather conditions for the three values of α . When the building is unoccupied, the deviation for all three curves remains close to 2°C below Δ_j , changing to 1°C below the temperature set-point during the hours of occupancy. The sudden reduction in temperature deviation values for $\alpha = 0.6$ and $\alpha = 1$ may be attributed to the pre-heating operation seen earlier in Fig. 4.

Fig. 6 shows the trend of power consumption for the three values of α on a typical winter day in Austin, TX. The pre-heating operation for $\alpha = 0$ and $\alpha = 0.6$ in anticipation of an increase in energy prices may be seen here as well. However, the spikes in power consumption are shorter than those observed in Fig. 4, owing to lower demand and energy prices. The power consumption levels progressively fall as the ambient temperatures increase between 0900 hrs and 1700 hrs, thereby reducing the heating power demand. A subsequent decrease in ambient temperatures after 1800 hrs results in a steady increase in power consumption for all values of α .

Figs. 4 and 6 show that the ECDCM strategy for $\alpha = 0$ significantly reduced the instantaneous power consumption levels under both extreme and normal weather conditions. Table II, which records the peak-to-average-power ratio (PAPR) for the three values of α under both extreme and normal weather conditions, further delineates the potential of the

Average temperature deviation (normal weather conditions)

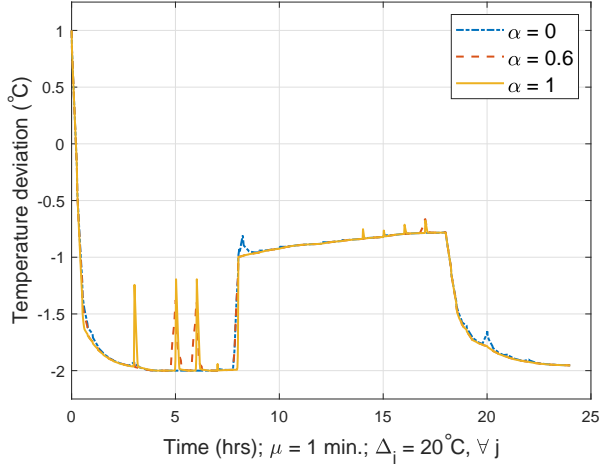


Fig. 7: Deviation from the temperature set-point for $\alpha = 0$, $\alpha = 0.6$ and $\alpha = 1$ under normal weather conditions, averaged for all six units in the commercial building.

ECDCM strategy in safeguarding the power grid infrastructure by minimizing the instantaneous peak power drawn by the commercial building. This indicates that the ECDCM strategy is robust to extreme changes in the ambient and can therefore be used to significantly reduce power demand peaks for a variety of load patterns and energy pricing signals.

TABLE II: Peak-to-average-power ratio values for ECDCM under extreme and normal weather conditions in Austin, TX.

| Weather | $\alpha = 0$ | $\alpha = 0.6$ | $\alpha = 1$ |
|---------|--------------|----------------|--------------|
| Extreme | 1.57 | 2.42 | 3.54 |
| Normal | 2.71 | 4.32 | 5.38 |

Fig. 7 shows the average deviation from Δ_j in the commercial building for the three values of α on a typical winter day in Austin, TX. As in Fig. 5, the curves for $\alpha = 0.6$ and $\alpha = 1$ exhibit the pre-heating operation in response to increasing energy prices. However, unlike Fig. 5, the average deviation gradually decreases from 1°C below Δ_j during the hours of occupancy. This behavior could be attributed to the fact that unit 6 in Fig. 2 is thermally coupled to the other five units that are being heated by the hydronic system. The ambient temperatures steadily increase during the hours of occupancy and are also significantly higher than those seen for extreme weather conditions in Fig. 3. Hence, the ambient and the spaces adjoining unit 6 drive the indoor temperatures to increase. This causes the average deviation from Δ_j between 0800 and 1800 hrs to steadily decrease, until the building is no longer occupied. Notice that we did not observe this behavior for extreme weather conditions as in that case the internal HVAC operations of the commercial building counteracted the falling ambient temperatures.

C. Performance Evaluation for Varying System Parameters (Cooling Operation)

July 20th, 2019 was observed to be the hottest day of the year in Albany, NY [23], with maximum ambient temperatures

Ambient temperature

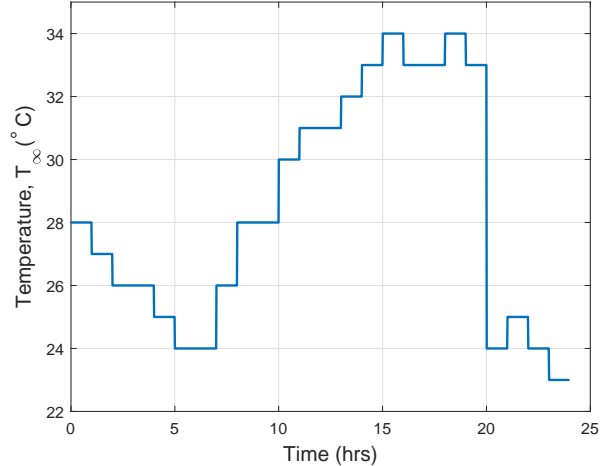


Fig. 8: Ambient temperature over a 24-hour period for a summer day in Albany, NY.

Total power consumed for varying values of α

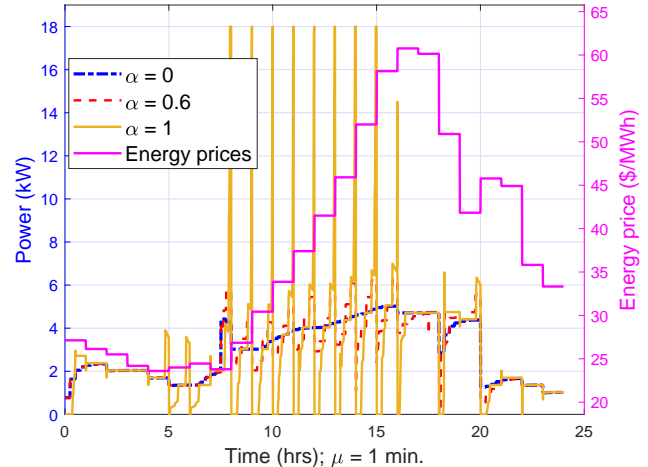


Fig. 9: Total power consumed by the building for $\alpha = 0$, $\alpha = 0.6$ and $\alpha = 1$ for Albany, NY, and the hourly energy pricing signals.

reaching 34°C . Our numerical study uses the hourly recorded ambient temperatures observed during that day (see Fig. 8) [24]. These values helped us evaluate the performance of our control strategy for cooling under high energy demand. We use hourly energy prices as promulgated by the New York independent system operator (NYISO) for July 20th, 2019 [25]. The value of ϖ in this study is $\$9.3/\text{kW}$, which is the mean of the DC tariffs charged by all utilities in NY [26]. As before, we assume that the tariffs are known (or are well-estimated) in advance.

Fig. 9 shows how the total power consumed by the hydronic HVAC system operating under the ECDCM strategy varies during the day, given hourly pricing signals. It is noteworthy that between 0000 and 0500 hrs both the ECs and the ambient temperatures progressively decrease. Hence, the power consumed by the commercial building exhibits a decreasing trend for all values of α under consideration. Subsequently, an increase in hourly energy prices is preceded by instances of very high power consumption of approximately 18 kW for

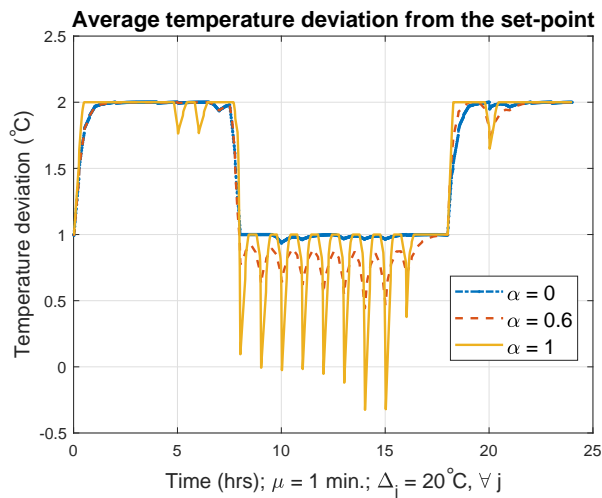


Fig. 10: Temperature deviation for $\alpha = 0$, $\alpha = 0.6$ and $\alpha = 1$, averaged for all six units in the commercial building.

$\alpha = 1$. These spikes in power consumption are followed by brief periods when the system consumes very little power. These measures are aimed at pre-cooling the units prior to an increase in energy prices, thereby reducing power consumption during the intervals with higher energy prices. The building's DR-amenability ensures that the indoor temperatures remain within permissible bounds even after this cost-saving mechanism takes effect. However, these brief periods of high power consumption result in an elevated DC. While the scenario with $\alpha = 0.6$ also involves minimizing DC, this pre-cooling action is seen to be less pronounced. Finally, no pre-cooling takes place for $\alpha = 0$ as this strategy is agnostic to changes in energy prices. The curve for $\alpha = 0$ does, however, show a sharp increase just before 0800 hrs, which is when the space is signaled to be occupied and when ρ is reduced to 1°C from 2°C .

Fig. 10 shows the temperature deviation from Δ_j (averaged over all units) when $\alpha = 0$, $\alpha = 0.6$ and $\alpha = 1$. It may be observed that for all three values of α , the temperature deviation remains close to $\rho = 1^\circ\text{C}$ during periods of occupancy. This deviation is closer to $\rho = 2^\circ\text{C}$ when the building is not occupied. Thus, the commercial building's DR-amenability allows the proposed control strategies to save energy without significantly compromising on the occupants' comfort. Furthermore, the control strategies using $\alpha = 0.6$ and $\alpha = 1$ utilize a pre-cooling mechanism to reduce power consumption during intervals with higher energy prices. This operation is reflected in a reduction in temperature deviation from the set-point for the two control strategies prior to increases in energy prices. Since $\alpha = 0$ makes the strategy impervious to energy prices, the HVAC system has no incentive to pre-cool the space. Therefore, $\alpha = 0$ does not demonstrate any notably sharp changes in temperature deviation.

Next, we determine how our performance metrics are affected by changing α , for given $\pi(\cdot)$ and ϖ . Table III records these changes. Since the power meter records an average power flow for each 15-minute interval, the DC payable by the customer is based on the largest average 15-minute power

flow during the billing period [27]. Therefore, Table III records this average power flow and multiplies it by ϖ to give the DC to be paid by the consumer. We assume that the particular day being considered here results in the largest load encountered by the building. As a simplification, we also assume that the daily energy consumption is identical throughout the month. The baseline represents the scenario where $\rho = 0$. The data for the monthly ECs represents the amount to be paid by the consumer for the energy consumed during the month, based on the per-unit energy prices. Lastly, the average temperature deviation represents the deviation of the mean temperature of all six units from Δ_j averaged over the entire 24-hour period.

It may be observed in Table III that as α increases, the ECs incurred by the consumer decrease. Additionally, increasing α also causes the pre-cooling action to be more drastic. Therefore, the largest average 15-minute power flow, Λ , and hence the DC, increase in magnitude with increase in α . Given the tariff structure considered here, the decrease in EC for increasing α does not compensate for the increase in DC. Since the DC dominates the total utility bill in this case, therefore, a general increase in the consumer's monthly bill may be observed for increasing α . This trend reinforces our motivation to minimize Λ along with the ECs incurred. Moreover, as the baseline scenario aims to strictly maintain the temperature set-point, therefore, it consumes the greatest energy of all the cases considered here. Since the baseline is not DR-amenable, it does not result in any pre-cooling action. Consequently, the DC for the baseline is significantly lower than those for higher values of α . We define % financial savings as the ratio of the difference between the total utility bills for the baseline and the ECDCM strategy for a particular value of α , to the total utility bill for the baseline. The results show that the % financial savings progressively decreases for $\alpha > 0.2$ due to a concomitant increase in the DC. Beyond $\alpha = 0.6$, the proposed strategy does not result in any savings.

D. Performance Evaluation for Various Climate Zones (Cooling Operation)

In this subsection, we determine the performance of the ECDCM strategy for different climate zones and tariff structures. We consider the climate zones prevalent in the US, with each zone being represented by the weather conditions of a certain region. Table IV shows the climate zones considered in this study, along with on-peak, partial peak and off-peak energy prices. The table also shows the average daily temperature, \bar{T} , for each zone and the corresponding demand charge, ϖ . Fig. 11 shows the ambient temperatures considered for each of the zones in Table IV [28]. Albany, NY, which represents the 'Cold' climate zone has already been studied in the preceding subsection. Here, we run our control strategy for $\alpha = 0$, $\alpha = 0.2$ and $\alpha = 1$ using representative values for $\pi(\cdot)$ and ϖ based on data for local utilities available online. We include the performance of $\alpha = 0.2$ as this value resulted in the lowest utility bill in Table III. Moreover, it is also worth studying if using $\alpha = 0.2$ remains the most economical approach for other climate zones as well. The on-peak hours

TABLE III: Performance evaluation of the ECDCM strategy for varying values of α .

| | Baseline | $\alpha = 0$ | $\alpha = 0.2$ | $\alpha = 0.4$ | $\alpha = 0.6$ | $\alpha = 0.8$ | $\alpha = 1$ |
|---|----------|--------------|----------------|----------------|----------------|----------------|--------------|
| I - Monthly energy consumed (kWh) | 2318 | 1964 | 1964 | 1963 | 1962 | 1950 | 1894 |
| II - Monthly energy cost (\$) | 94.2 | 81.0 | 81.0 | 80.7 | 80.2 | 79.4 | 76.9 |
| III - Peak 15-min. power flow (kW) | 5.36 | 5.02 | 5.02 | 5.87 | 6.17 | 8.36 | 9.78 |
| IV - Demand charge (\$) [III \times ϖ] | 49.9 | 46.7 | 46.7 | 54.6 | 57.4 | 77.8 | 90.9 |
| V - Total utility bill [II + IV] (\$) | 144.1 | 127.7 | 127.6 | 135.5 | 137.6 | 157.2 | 167.8 |
| VI - % financial savings | - | 11.38 | 11.45 | 5.97 | 4.51 | -9.09 | -16.45 |
| VII - Avg. temperature deviation ($^{\circ}$ C) | 0 | 1.55 | 1.53 | 1.50 | 1.45 | 1.44 | 1.47 |

TABLE IV: Climate zones with representative energy prices and DC tariffs.

| Climate zone | Region | Energy Price (\$/MWh) | | | \tilde{T} ($^{\circ}$ C) | ϖ (\$/kW) |
|--------------|----------------|-----------------------|---------|-------|-----------------------------|------------------|
| | | On | Partial | Off | | |
| Hot-Dry | Sacramento, CA | 232.2 | 177.1 | 149.0 | 30.1 | 11.45 |
| Marine | Portland, OR | 61.91 | - | 46.91 | 26.5 | 2.61 |
| Very Cold | Juneau, AK | - | - | 59.2 | 21.7 | 13.85 |
| Hot-Humid | Austin, TX | 65.73 | - | 28.4 | 30.9 | 4.19 |
| Mixed-Humid | Raleigh, NC | 145 | - | 59.5 | 28.7 | 15.61 |
| Mixed-Dry | Lincoln, NM | 30.22 | - | 15.7 | 23.1 | 25.61 |

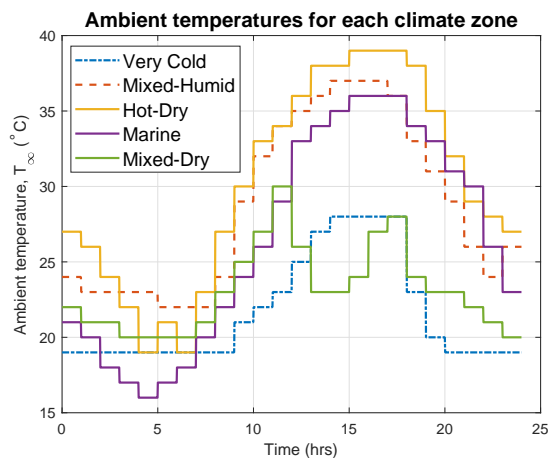


Fig. 11: The ambient temperatures considered for the climate zones in this section.

for the Hot-Dry climate zone are between 1200 hrs and 1800 hrs, whereas the intervals 0830-1200 hrs and 1800-2130 hrs represent partial peak hours. An off-peak energy price is levied for the rest of the day. The on-peak hours for the Marine climate zone are between 1600 hrs and 2000 hrs, for the Hot-Humid climate zone between 1600 hrs and 1800 hrs, for the Mixed-Humid climate zone between 1400 hrs and 2000 hrs, and for the Mixed-Dry climate zone between 0800 hrs and 2000 hrs. Finally, the energy prices for the Very Cold zone remain flat for the entire 24-hour period. The ambient temperatures are based on the hottest days recorded in the respective cities in 2019 [28]. Our primary objective here is to determine the effect of changing α on the energy consumption, peak demand and the amount payable to the utility for these climate zones. Each of the aforementioned zones represent the full range of power demands for thermal regulation during a 24-hour period – from high (Hot-Humid) to intermediate (Marine) to low (Very Cold).

Table V records the performance of our power control strategy for $\alpha = 0$, $\alpha = 0.2$ and $\alpha = 1$ for Hot-Dry, Marine and Very Cold climate zones. The DC, the total utility

bill and the % financial savings compared to the baseline have been determined in the same manner as in Subsection V-C. As expected, the energy consumed for thermal regulation increases with increase in \tilde{T} in Table IV. It is noteworthy that although the energy consumption for $\alpha = 0.2$ in the Hot-Dry climate zone is higher than that for $\alpha = 0$, the former results in a lower monthly EC than the latter. This trend may be attributed to the pre-cooling action seen for $\alpha > 0$. It may also be seen that the ambient temperature and the tariff structure affect the peak power consumption for all three values of α . For instance, the values of Λ recorded for the Very Cold climate are the lowest among the three climate zones being studied. Furthermore, since this climate zone, unlike the other two, uses a flat energy pricing scheme the power control scheme with $\alpha = 1$ does not pre-cool the indoor spaces. Hence, there is no appreciable difference in Λ for the three values of α for this climate zone. In fact, without hourly or time-of-use pricing, it can be inferred that the DC incurred for the three values of α studied here is not drastically different from that incurred for the baseline. Hence, unlike the rest of the climate zones studied here, the disparity in the monthly utility bills between the baseline and the system using ECDCM in the Very Cold zone can be attributed to the difference in ECs in the two cases. Therefore, the DR-amenable of our system results in significant savings in the Very Cold climate zone as compared to the other two zones. Moreover, % financial savings with respect to the baseline case for Hot-Dry and Marine climate zone tends to decrease with increasing value of α . Finally, the average temperature deviation is observed to be lower for cooler climates. This is because the temperature gradient between the ambient and the indoor space is less steep for climate zones with lower \tilde{T} . Therefore, less heat moves from the surroundings to the indoor space. This also results in less demand for space cooling.

Table VI records the performance of the ECDCM strategy for $\alpha = 0$, $\alpha = 0.2$ and $\alpha = 1$ for Hot-Humid, Mixed-Humid and Mixed-Dry climate zones. As noted earlier, the energy cost for $\alpha = 1$ remains the lowest for all three values of α considered in Table VI. Other than the Mixed-Humid climate zone, Λ and hence the DC, generally increase for increasing values of α . In the case of the Mixed-Humid climate zone, Λ was seen to be higher for $\alpha = 0.2$ than $\alpha = 1$. However, the maximum *instantaneous* power consumption for $\alpha = 0.2$ was seen to be lower than that for $\alpha = 1$, as indicated by the corresponding PAPR values. It may further be seen in the table that since the Mixed-Dry zone has the lowest \tilde{T} of the

TABLE V: Performance evaluation of the ECDCM strategy for $\alpha=0$, $\alpha=0.2$ and $\alpha=1$ for various climate zones and tariff structures.

| | Hot-Dry | | | | Marine | | | | Very Cold | | | |
|---------------------------------|----------|------------|--------------|------------|----------|------------|--------------|------------|-----------|------------|--------------|------------|
| | Baseline | $\alpha=0$ | $\alpha=0.2$ | $\alpha=1$ | Baseline | $\alpha=0$ | $\alpha=0.2$ | $\alpha=1$ | Baseline | $\alpha=0$ | $\alpha=0.2$ | $\alpha=1$ |
| Monthly energy consumed (kWh) | 2701 | 2391 | 2397 | 2375 | 1924 | 1668 | 1670 | 1669 | 860 | 621 | 618 | 616 |
| Monthly energy cost (\$) | 524.27 | 470.80 | 468.90 | 465.30 | 99.68 | 86.48 | 85.74 | 85.74 | 50.89 | 36.77 | 36.57 | 36.44 |
| PAPR | 1.83 | 1.89 | 3.52 | 5.09 | 1.05 | 2.41 | 10.72 | 14.46 | 1.10 | 3.51 | 3.53 | 5 |
| Peak 15-min. power flow (kW) | 7.36 | 6.75 | 10.06 | 11.42 | 6.35 | 5.73 | 9.82 | 11.44 | 3.64 | 3.02 | 3.02 | 3.05 |
| Demand charge (\$) | 80.72 | 77.29 | 115.19 | 130.76 | 15.75 | 14.97 | 25.64 | 29.87 | 45.72 | 41.89 | 41.89 | 42.20 |
| Total utility bill (\$) | 604.99 | 548.09 | 584.09 | 596.06 | 115.43 | 101.45 | 111.38 | 115.61 | 96.61 | 78.66 | 78.46 | 78.64 |
| % financial savings | - | 9.40 | 3.45 | 1.47 | - | 12.10 | 3.50 | -0.16 | - | 18.59 | 18.80 | 18.61 |
| Avg. temperature deviation (°C) | 0 | 1.47 | 1.45 | 1.47 | 0 | 1.11 | 0.96 | 0.99 | 0 | 0.80 | 0.82 | 0.82 |

three climate zones, its monthly energy consumption, as well as the average temperature deviation is also the lowest among the three climate zones.

E. Impact of Ignoring Thermal Coupling on ECDCM's Performance

As stated previously, we have incorporated thermal coupling into the optimization framework to account for heat transfer among the indoor units. We now present results for the performance evaluation of the ECDCM strategy for the Hot-Humid climate zone when thermal coupling among the indoor spaces is ignored and heat transfer is only assumed to take place between the ambient and the individual units. Table VII summarizes our findings and records the % difference from the corresponding readings in Table VI. As can be seen in this table, ignoring heat transfer between adjoining zones can lead to major over-estimates for the energy consumption levels for each value of α . Therefore, the simulation results in Table VII are indicative of the significance of considering thermal coupling for the performance evaluation for building HVAC control policies.

F. Impact of Forecast Errors in Pricing on ECDCM's Performance

The simulation results in the preceding subsections assumed that the energy prices for each climate zone were known or were well-estimated in advance. However, in reality, there may be significant errors in forecasting the energy prices to be used in the ECDCM strategy. In order to simulate the errors in estimating the energy prices in advance, we introduce Gaussian noise in the energy prices used for simulating the performance for ECDCM strategy for the Hot-Humid climate zone.

Table VIII shows how errors in forecasting can affect the monthly energy costs for implementing the ECDCM strategy to the commercial building. It may be seen that the deviation of the monthly energy costs from Table VI remains within 2% in each case.

Table IX shows the impact of under-estimating energy prices during the implementation of the ECDCM strategy. Here, it may be seen that for the Hot-Humid climate zone, under-estimating the energy prices due to Gaussian noise with a standard deviation of 10% caused the monthly energy costs for implementing the ECDCM strategy to increase by less than 5% as compared to the results in Table VI.

G. Comparison with m-AHC

Table X tabulates the energy consumption and the financial costs incurred when the m-AHC approach is used to implement EC and peak power control. The table also shows how the performance of the m-AHC approach for these indicators compares with that of ECDCM as recorded in Table VI. It may be seen that the ECDCM approach can potentially offer financial savings of up to 6.14% as compared to the m-AHC approach.

In order to ascertain the scalability of the ECDCM strategy, we simulated the execution times of optimizing the weighted sum of the peak power consumption and the energy costs over a 37-minute window as the number of units increases significantly. Fig. 12 shows the time taken to generate the solution for the ECDCM and m-AHC approaches for an increasing number of units. A large number of indoor units can represent the scenario where our proposed strategy is implemented for a fleet of commercial buildings. compares the execution times for the ECDCM and m-AHC strategies for an increasing number of indoor units. The figure shows that as the number of units increases to 240, which is 40 times the number of units considered in our paper, there is only a 35% increase in the execution times for the ECDCM strategy. In contrast, for m-AHC, when the number of units becomes 12 times the number of units considered in our paper, the execution times are more than 7 times that seen for ECDCM. This observation is primarily due to the fact that the m-AHC implements peak power control in two stages which significantly adds to the computational overhead of the algorithm. Therefore, it can be concluded that based on the computation times alone, our control strategy can be used to jointly optimize the energy costs and peak power consumption in a large group of 6-indoor unit commercial buildings.

VI. CONCLUSION

In this work, we developed a control framework for a hydronic HVAC system of a multi-unit commercial building. We determined the optimal power flow to the building that minimized the weighted sum of EC and the peak power consumption in a commercial building. We developed mathematical expressions for modeling the temperature evolution in the building over time and showed how the problem can be transformed into a linearly-constrained, convex optimization problem. We ran simulations to determine the instantaneous, optimal power consumption for known ambient conditions and tariff structures. We assessed our control policy's performance

TABLE VI: Performance evaluation of the ECDCM strategy for $\alpha=0$, $\alpha=0.2$ and $\alpha=1$ for various climate zones and tariff structures.

| | Hot-Humid | | | | Mixed-Humid | | | | Mixed-Dry | | | |
|---|-----------|------------|--------------|------------|-------------|------------|--------------|------------|-----------|------------|--------------|------------|
| | Baseline | $\alpha=0$ | $\alpha=0.2$ | $\alpha=1$ | Baseline | $\alpha=0$ | $\alpha=0.2$ | $\alpha=1$ | Baseline | $\alpha=0$ | $\alpha=0.2$ | $\alpha=1$ |
| Monthly energy consumed (kWh) | 2880 | 2509 | 2395 | 2370 | 2367 | 2040 | 2048 | 2020 | 1097 | 858 | 858 | 854.6 |
| Monthly energy cost (\$) | 95.83 | 82.94 | 80.72 | 79.50 | 223.13 | 195.63 | 191.76 | 189.98 | 29.29 | 23.23 | 23.23 | 23.06 |
| PAPR | 1.56 | 2.04 | 3.63 | 4.74 | 1.80 | 2.38 | 4.14 | 6.20 | 2.38 | 3.00 | 3.04 | 12.64 |
| Peak 15-min. power flow (kW) | 6.69 | 6.41 | 10.23 | 11.67 | 6.35 | 6.07 | 11.47 | 10.15 | 3.88 | 3.57 | 3.63 | 5.60 |
| Demand charge (\$) | 28.02 | 26.86 | 42.87 | 48.91 | 99.11 | 94.79 | 178.98 | 158.42 | 99.26 | 91.53 | 92.84 | 143.32 |
| Total utility bill (\$) | 123.85 | 109.80 | 123.59 | 128.41 | 322.24 | 290.43 | 370.74 | 348.40 | 128.55 | 114.76 | 116.07 | 166.38 |
| % financial savings | - | 11.35 | 0.21 | -3.68 | - | 9.85 | -15.05 | -8.12 | - | 10.72 | 9.66 | -29.43 |
| Avg. temperature deviation ($^{\circ}\text{C}$) | 0 | 1.62 | 1.54 | 1.58 | 0 | 1.55 | 1.53 | 1.57 | 0 | 1.29 | 1.30 | 1.29 |

TABLE VII: Performance evaluation of the ECDCM strategy for $\alpha=0$, $\alpha=0.2$ and $\alpha=1$ when thermal coupling is ignored for Hot-Humid climate zone.

| | Baseline | % Difference from Table VI | $\alpha = 0$ | % Difference from Table VI | $\alpha = 0.2$ | % Difference from Table VI | $\alpha = 1$ | % Difference from Table VI |
|---|----------|----------------------------|--------------|----------------------------|----------------|----------------------------|--------------|----------------------------|
| Monthly energy consumed (kWh) | 7014 | 143.5 | 7011 | 179.2 | 6529 | 172.6 | 6529 | 175.5 |
| Monthly energy cost (\$) | 226.3 | 136.2 | 226.2 | 172.7 | 210.2 | 160.4 | 210.2 | 164.4 |
| Peak 15-min. power flow (kW) | 12.84 | 91.93 | 12.83 | 100.2 | 12.83 | 25.42 | 13.17 | 12.85 |
| Demand charge (\$) | 53.78 | 91.93 | 53.77 | 100.2 | 53.77 | 25.42 | 53.77 | 9.94 |
| Total utility bill (\$) | 280.01 | 126.1 | 279.97 | 155.0 | 263.97 | 113.6 | 263.97 | 105.6 |
| Avg. temperature deviation ($^{\circ}\text{C}$) | 0 | 0 | 1.00 | -38.3 | 1.23 | 25.20 | 1.61 | 1.90 |

TABLE VIII: Monthly energy costs for the ECDCM strategy for $\alpha=0$, $\alpha=0.2$ and $\alpha=1$ for varying forecast errors in pricing for Hot-Humid climate zone.

| Standard Deviation | $\alpha = 0$ | % Difference from Table VI | $\alpha = 0.2$ | % Difference from Table VI | $\alpha = 1$ | % Difference from Table VI |
|--------------------|--------------|----------------------------|----------------|----------------------------|--------------|----------------------------|
| 2% | 82.89 | -0.060 | 79.48 | -1.54 | 78.84 | -0.830 |
| 5% | 83.01 | 0.084 | 79.36 | -1.68 | 78.83 | -0.843 |
| 10% | 82.63 | -0.374 | 79.57 | -1.42 | 78.68 | -1.03 |

TABLE IX: Monthly energy costs for the ECDCM strategy for $\alpha=0$, $\alpha=0.2$ and $\alpha=1$ for when energy prices for the Hot-Humid climate zone are under-estimated during simulation.

| Standard Deviation | $\alpha = 0$ | % Difference from Table VI | $\alpha = 0.2$ | % Difference from Table VI | $\alpha = 1$ | % Difference from Table VI |
|--------------------|--------------|----------------------------|----------------|----------------------------|--------------|----------------------------|
| 2% | 83.76 | 0.988 | 80.24 | 0.111 | 79.60 | 0.126 |
| 5% | 85.00 | 2.48 | 81.51 | 0.979 | 80.75 | 1.57 |
| 10% | 87.04 | 4.90 | 83.48 | 3.42 | 82.74 | 4.08 |

TABLE X: Performance evaluation for the m-AHC strategy for $\alpha=0$ and $\alpha=1$ and its comparison with ECDCM for the Hot-Humid climate zone.

| | $\alpha = 0$ | % Difference from Table VI | $\alpha = 1$ | % Difference from Table VI |
|-------------------------------|--------------|----------------------------|--------------|----------------------------|
| Monthly energy consumed (kWh) | 2698.6 | 7.56 | 2388.1 | 0.764 |
| Monthly energy cost (\$) | 90.04 | 8.56 | 79.77 | 0.34 |
| Demand charge (\$) | 27.27 | 1.53 | 56.57 | 15.7 |
| Total utility bill (\$) | 111.2 | 1.28 | 136.3 | 6.14 |

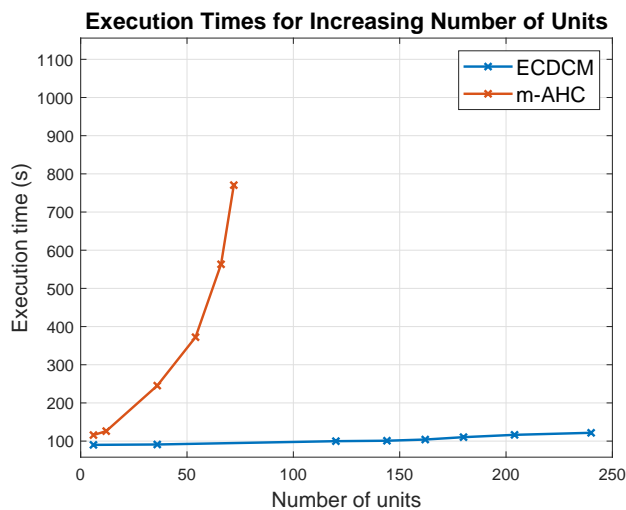


Fig. 12: Execution times for the ECDCM and the m-AHC approaches for increasing number of indoor units.

for both normal and anomalous weather events and noted that it has the potential for significantly reducing peak power consumption in GEBs. Finally, we tested our control strategy under various demand scenarios for hourly, on-peak-off-peak and flat energy pricing strategies. Our results showed that the proposed approach has a strong potential for saving significant electricity cost. This control policy can be extended to include various grid services, e.g. frequency regulation, with different temporal granularities. This extension is left as future work.

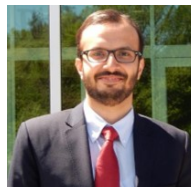
VII. ACKNOWLEDGMENTS

This work was supported by the National Science Foundation through Award No. 1827546.

REFERENCES

- [1] U.S. Department of Energy, "Energy savings potential and RD & D opportunities for commercial building HVAC systems," Dec. 2017, [Online] Available: <https://www.energy.gov/sites/prod/files/2017/12/f46/bto-DOE-Comm-HVAC-Report-12-21-17.pdf>.

- [2] "Understanding demand charges," [Online] Available: <https://www.nyserda.ny.gov/All-Programs/Programs/Energy-Storage/Energy-Storage-for-Your-Business/Understanding-Demand-Charges>.
- [3] N. Fernandez *et al.*, "Energy savings modeling of re-tuning energy conservation measures in large office buildings," in *Journal of Building Performance Simulation*, vol. 8, no. 6, pp. 391-407, 2014.
- [4] M. Piette, D. Watson, N. Motegi and S. Kiliccote, "Automated critical peak pricing field tests: 2006 pilot program description and results," *LBNL-59351*, 2007.
- [5] P. Hohne, K. Kusakana, and B. Numbi, "Improving energy efficiency of thermal processes in healthcare institutions: A review on the latest sustainable energy management strategies," *Energies*, vol. 13, no. 3, p. 569, Jan. 2020.
- [6] U.S. Department of Energy, "Grid-interactive efficient buildings," Apr. 2019, [Online] Available: energy.gov/sites/prod/files/2019/04/f61/bto-geb_overview-4.15.19.pdf.
- [7] M. Ali, J. Jokisalo, K. Siren, and M. Lehtonen, "Combining the demand response of direct electric space heating and partial thermal storage using LP optimization," in *Electric Power System Research*, vol. 106, pp. 160-167, Jan. 2014.
- [8] S. Naqvi, K. Kar, S. Bhattacharya and V. Chandan, "Peak power reduction for HVAC Operations in multi-unit commercial buildings," in *Proc. IEEE Power & Energy Society Innovative Smart Grid Technologies Conference (ISGT)*, 2021, pp. 01-05.
- [9] Y. Wang, Y. Tang, Y. Xu and Y. Xu, "A distributed control scheme of thermostatically controlled loads for the building-microgrid community," in *IEEE Trans. Sustain. Energy*, vol. 11, no. 1, pp. 350-360, Jan. 2020.
- [10] J. Wang, S. Huang, D. Wu and N. Lu, "Operating a commercial building HVAC load as a virtual battery through airflow control," in *IEEE Trans. Sustain. Energy*, vol. 12, no. 1, pp. 158-168, Jan. 2021.
- [11] S. Sharma, A. Verma, Y. Xu and B. Panigrahi, "Robustly coordinated bi-level energy management of a multi-energy building under multiple uncertainties," in *IEEE Trans. Sustain. Energy*, vol. 12, no. 1, pp. 3-13, Jan. 2021.
- [12] Y. Lu *et al.*, "Bi-level optimization framework for buildings to heating grid integration in integrated community energy systems," in *IEEE Trans. Sustain. Energy*, vol. 12, no. 2, pp. 860-873, April 2021.
- [13] X. Jin, Q. Wu, H. Jia and N. Hatziaargyriou, "Optimal integration of building heating loads in integrated heating/electricity community energy systems: A bi-level MPC approach," in *IEEE Trans. Sustain. Energy*, vol. 12, no. 3, pp. 1741-1754, July 2021.
- [14] M. Avci, M. Erkocand, and S. Asfour, "Residential HVAC load control strategy in real-time electricity pricing environment," in *Proc. IEEE Energytech*, May 2012, pp.1-6.
- [15] A. Vishwanath, V. Chandan, and K. Saurav, "An IoT-based data driven precooling solution for electricity cost savings in commercial buildings," in *IEEE Internet Things J.*, vol. 6, no. 5, Oct. 2019.
- [16] J. Mei and X. Xia, "Multi-zone building temperature control and energy efficiency using autonomous hierarchical control strategy," in *Proc. IEEE International Conference on Control and Automation (ICCA)*, Jun. 2018, pp. 884-889.
- [17] T. Wei, M. Islam, S. Ren and Q. Zhu, "Co-scheduling of datacenter and HVAC loads in mixed-use buildings," in *Proc. International Green and Sustainable Computing Conference (IGSC)*, Nov. 2016, pp. 1-8.
- [18] H. Sane and M. Guay, "Minmax dynamic optimization over a finite-time horizon for building demand control," in *Proc. American Control Conference (ACC)*, 2008, pp. 1469-1474.
- [19] S. Naqvi, K. Kar, S. Bhattacharya and V. Chandan, "Optimizing HVAC operations in multi-unit buildings for grid demand response," in *Proc. American Control Conference (ACC)*, Jul. 2020, pp. 2333-2338.
- [20] "Nonhomogeneous linear systems of differential equations with constant coefficients," [Online] Available: <http://people.math.gatech.edu/~xchen/teach/ode/NonhomoSys.pdf>.
- [21] M. Minakais, S. Mishra, J. T. Wen, L. Lagace, and T. Castiglia, "Design and instrumentation of an intelligent building testbed," in *Proc. IEEE Int. Conf. Automat. Sci. Eng. (CASE)*, Gothenburg, Sweden, Aug. 2015, pp. 1-6.
- [22] Z. Tariq, K. Kar, S. Mishra and J. Wen, "Enabling better thermal management of indoor spaces through adaptive zonal heat transfer," *Annual American Control Conference (ACC)*, Milwaukee, WI, 2018, pp. 5418-5423.
- [23] "Jason Gough: Hottest part of the day will stretch from 12 to 8 p.m.," [Online] Available: <https://www.timesunion.com/news/article/Jason-Gough-Hottest-part-of-the-day-will-stretch-14110334.php>.
- [24] "Weather in July 2019 in Albany, New York, USA," [Online] Available: <https://www.timeanddate.com/weather/usa/albany-ny/historic?month=7&year=2019>.
- [25] "Day-Ahead Market LBMP - Zonal", [Online] Available: <http://mis.nyiso.com/public/P-2A1ist.html>.
- [26] National Renewable Energy Laboratory (NREL), "A Survey of U.S. demand charges," Sep. 2017.
- [27] Northwestern Energy, "Demand charges explained," [Online] Available: <https://www.northwesternenergy.com/docs/default-source/documents/E-Programs/E-demandcharges.pdf>.
- [28] [Online] Available: <https://www.wunderground.com/history>.
- [29] https://www.dropbox.com/s/wg6bwfym8mp4603/SE_TechReport.pdf



Syed Ahsan Raza Naqvi (Student Member, IEEE) received the B.S. degree in electrical engineering from the National University of Sciences and Technology (NUST), Pakistan, in 2015, and the M.S. degree in electrical engineering from Rensselaer Polytechnic Institute, Troy, NY, USA, in 2019, where he is currently pursuing his Ph.D. degree. His research interests lie in the general areas of optimal control for cyber-physical systems and the internet-of-things. Specifically, he is interested in energy efficient personalized climate control and indoor air quality management in buildings and energy markets.



Dr. Koushik Kar is a Professor in the Electrical, Computer & Systems Engineering department at Rensselaer Polytechnic Institute, Troy, NY, where he has been a faculty member since 2002. Dr. Kar's primary research interests include developing and analyzing low-complexity optimization algorithms and methods for Internet and wireless networks, smart buildings and the smart grid. He received his B.Tech. degree in Electrical Engineering in 1997 from the Indian Institute of Technology, Kanpur, and his M.S. and Ph.D. degrees in Electrical & Computer Engineering from the University of Maryland, College Park, in 1999 and 2002, respectively. Dr. Kar received the Career Award from the National Science Foundation in 2005, and won multiple best paper awards in international journals and conferences.



Saptarshi Bhattacharya (S'12-M'18) obtained his M.S. and Ph.D. (all in Electrical Engineering) from Rensselaer Polytechnic Institute, Troy, NY, USA in 2014 and 2018 respectively. Since 2018, he has been a research staff member at Pacific Northwest National Laboratory (PNNL), Richland, WA. His research interests are in all aspects of modeling, analysis, optimization, and controls for cyber-physical energy systems. Specific topics of interests include transactive energy systems, building controls and performance optimization, renewable energy integration and power system economics. He is member of the IEEE, IEEE Power and Energy Society, IEEE Control Systems Society

and INFORMS. He is also a regular reviewer for various top-tier conferences and journals, including American Control Conference (ACC), IEEE PES General Meeting, ISGT, IEEE Transactions on Smart Grid, IEEE Transactions on Sustainable Energy, IEEE Transactions on Power Systems, IEEE Transactions on Control Syst. Technol., Applied Energy, etc.



Vikas Chandan is a Scientist and Team Leader in the Optimization and Control Group within the Energy and Environment Directorate at PNNL. His research specializes in the application of modeling, control and optimization to the area of energy systems, in particular building systems, with a recent emphasis on data driven techniques to support de-

carbonization goals. He is actively involved in efforts related to development of benchmark datasets for buildings, modeling and control of buildings to support grid interaction and transactive goals, Physics informed Machine Learning for Buildings, and demonstration of value provided by Machine Learning for buildings. Prior to joining PNNL, he was a Research Scientist at IBM Research from 2013 to 2016. He received his M.S. and Ph.D. degrees from the University of Illinois at Urbana-Champaign in 2010 and 2013 respectively.